Egypt. J. Chem. **Vol. 67**, No. 12 pp. 399 - 408 (2024)

Egyptian Journal of Chemistry

http://ejchem.journals.ekb.eg/

Practical Evaluation and Theoretical Modelling of Charging Process for Lead Acid Batteries in PV Systems

R. M. Abdo[a], Aiat Hegazy[a*], E. F. El-Sherbini[b], E. T. El Shenawy[a]

[a] *Solar Energy Department, National Research Center, Cairo, Egypt*

[b] *Chemistry Department, Faculty of Science, Ain Shams University, Cairo, Egypt*

Abstract

The growing population along with the socio-economic development has led to increased global electricity demand. Accordingly, there is a growing interest in PV systems as a viable solution to address this electricity shortage. Batteries play an important role not only in PV systems but also in the electrical and hybrid electric vehicle industries. Efficient power control and management of batteries are essential for ensuring the safety and optimal performance of PV systems and automotive industries. This paper has provided valuable insight into the charging process of lead-acid batteries across a wide range of states of charge (SOC%) to achieve significant improvements in battery technology and develop more efficient charging methods via the validation of the modified Thévenin model. The electric characteristics for the models were assessed as a function of SOC% to accurately represent battery performance while maintaining model simplicity, and enhancing model topology by establishing an accurate relationship between battery capacity or SOC% and voltage. Additionally, efforts were made to enhance the model topology by establishing an accurate relationship between battery capacity or SOC and voltage. The modified Thévenin model was experimentally validated on a 200 Ah lead acid battery at full charge (at approximately 100% SOC), resulting in a Root Mean Square Error (RMSE) of around 1%. This validates that the model effectively captures battery behavior across its entire operating range.

***Keywords*:** lead acid battery; Equivalent circuit model; Thévenin model; charging.

1. Introduction

In remote areas, the demand for standalone energy systems is increasing. The growing interest in renewable energy is driven by its availability and environmental benefits, not only in remote areas but also in modern societies [1–3]. Utilizing photovoltaic systems to address Egypt's electricity shortage issues is a major focus. Egypt receives a substantial amount of solar radiation of around 6.5 kWh/m²/day, similar to high levels received at the Sunbelt region [4]. Adopting and implementing PV systems can be seen as a feasible transition from fossil fuels to renewable energy for an electric power system [5–7].

Batteries, as energy storage units in photovoltaic (PV) systems, mitigate the intermittent and unpredictable nature of solar energy. As a result, battery performance greatly affects the system's overall efficiency and represents the largest portion of the system's total cost [3,8]. With the critical shift towards off-grid photovoltaic battery systems, understanding battery performance has become more crucial, increasing the demand for rigorous testing. These tests aim to subject the battery to conditions similar to or more demanding than actual use, to investigate its long-term behavior [9]. Lead-acid batteries (LAB) have achieved a level of maturity and are widely used in a range of engineering applications [10–15]. They continue to be the most prevalent choice for energy storage and delivery in PV systems due to their low cost. Their dominance over other storage technologies, such as Li-ion, is also due to their high recyclability, exceeding 95%, enabling the materials to be reused for new batteries [12, 13]. This recyclability paves the way for the advancement of technologies to make lead-acid batteries more cost-effective and environmentally

*Corresponding author e-mail: aiathussien@gmail.com (Aiat Hegazy)

EJCHEM use only: Received date 06 June 2024; revised date 13 July 2024; accepted date 14 July 2024

DOI: 10.21608/ejchem.2024.295727.9814

sustainable. Additionally, they boost a high power-to-weight ratio, particularly in terms of specific energy [16–18]. However, similar to other batteries, lead-acid batteries face various technical obstacles related to safety concerns, in addition to the difficulties in small-size battery manufacturing, and short-circuiting [18].

Unproficient operation and poor monitoring systems for lead-acid batteries may not only cause power loss and operational disruptions but also lead to potentially dangerous accidents. For instance, overcharging increases the internal temperature of the battery and may induce side reactions that result in fires and explosions [17]. Several parameters can affect the battery performance such as charging and discharging rates, depth of discharges, and temperature fluctuations [19–21]. Predicting the battery performance accurately is very difficult. This can be attributed to that the battery's operational conditions are not constant but vary in a wide range. Consequently, battery modeling and monitoring the rate of charge and discharge in addition to the state of charge of the battery is essential for the battery's safe operation and enhancement of the overall PV system performance [22].

Battery modeling can be considered a profitable method for comprehending the activity of a battery system. Such models involve developing mathematical equations and algorithms that capture the behavior and performance characteristics of batteries [19–21]. The objective of battery modeling is to simulate their voltage response, state of charge (SOC), and other important parameters under various operating conditions.

The most common battery models are Equivalent circuit models (ECM) which gained significant popularity owing to the fact that it balanced between both the accuracy and simplicity [23–25]. It allows a simplified representation of the battery characteristics where a detailed understanding of chemical mechanisms is not required. In addition, it represents the battery behavior with a set of easily measured electrical parameters thus avoiding the computational complexity [26–28]. The general construction of the EC models is a circuit composed of a voltage source in addition to resistors and capacitors [23, 29]. The earliest form of the ECMs was introduced by Kim and Ha et. al. [30]. However, significant progress has been made in the development of ECMs over the years [20,31–33]. Numerous proposals followed to help in the accurate description of the dynamic behavior. Considering the dependence of the electrical parameter of the EC (open circuit voltage, resistance and capacitors) on the SOC instead of being constant was one solution to help in describing the dynamic behavior [20,34]. Further developments were achieved by considering the nonlinear behavior of the EC parameters to increase the accuracy of the model without affecting its simplicity [35–38]. Though the addition of more R//C components to the EC can provide a better understanding of the battery kinetics like charge transfer, polarization, and ions diffusion, this will in turn increase the computational complexity and costs [26, 39–45]. In order to fulfill high-precision SOC estimation, ECMs were hybridized with different algorithms such as Neural network, Kalman, Gaussian, and supportive vector regression. etc. [25, 46–49]. Other authors used a different method to adjust the parameters for the sake of achieving a better precision of modeling. A set of discharge and charge pulses are employed for obtaining the initial values for battery parameters which are fitted with the remaining SOC [26,28,50]. This method along with the estimation algorithm meets the real simulation and engineering requirements owing to their rapid convergence and high prediction precision. The real-time dynamic battery simulation is easily predicted as well.

In the current study, we aim to better understand the charging process through modeling using an improved Thévenin model. By monitoring the charging process, we can gain valuable advancements in battery technology and get more efficient charging strategies

2. Methods

This section will outline the methodology, experimental protocols, and model validations using real battery data.

2.1. Experimental Set-up

2.1.1. Charging system Description

The main components of charging systems are the tested battery, charging units, and loads. In the present study, a gel-type Sonnenschein 412 lead-acid battery (12 V/200 Ah) was used as the tested battery. Two charging systems were designed; an off-grid PV system and an electricity grid-charging one, shown in Figures 1 and 2, respectively. In off-grid PV charging system, the battery was charged in a system consisting of two parallel connected Sunset-1406 solar modules (140 W, Isc ≈8.3A, Voc =21.8V) as the charging unit and Tarom 4545 (12/24 V– 45 A) charge controller. SPM-1116SD solar power meter was used to measure the solar radiation during the tested period. Multimeter is used to measure the battery voltage and a clamp meter (KEW2002PA KYORITSU) is used to measure the current passes during the charging process. In addition to the tested battery, the electricity-grid charging system was composed of a 0.6 kW SUVPR (12 V) inverter to convert the AC current from the grid into DC current, computable to the battery and equipment to measure the voltage and current.

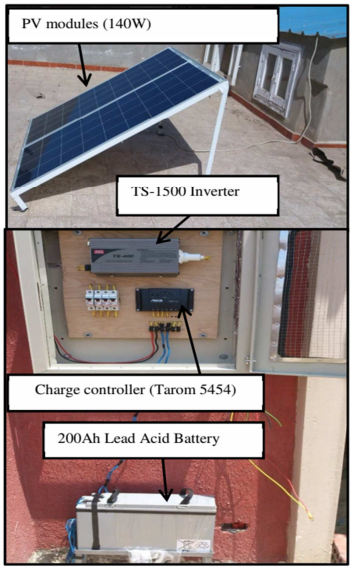

Figure 1: Installed off-grid PV charging system

Figure 2: installed Electricity-grid charging system

2.1.2. Methodology:

Throughout the charging tests, various parameters were measured. The charging unit parameters include solar irradiation, PV charging current, DC charging current converted by the inverter. The battery parameters are the terminal voltage, the current accepted by the battery, and the open circuit voltage. In the off-grid PV charging procedure, an off-grid system is constructed to study the effect of environmental parameters like solar radiation on the charging process of lead-acid batteries. The charging procedures took place in March 2021 for 6 hours/day during the daytime from 8:30 am to 2:30 pm. During this duration, the maximum solar energy intensity is guaranteed, allowing for an electrical current within the range of 6 to 9 Amperes. The charging current for this system ranged from 7-8 A (≈C/25). To calculate the improved Thévenin model parameters, it was necessary to perform the charging process utilizing a constant current supply. For this purpose, an electricity-grid charging system was constructed. In the electricity-grid charging, the battery was charged through a pulse-charge process involving repeated charging steps for 30 minutes with 8 A within the 20-100 % SOC range. Each charging step was followed by a 45-minute rest period. In order to test the model validity in our system, the voltage of the battery was simulated from pulse-charge tests through the determination of the EC's electric parameters. The relation between these parameters and SOC was fitted resulting in equations incorporated into the simulation model.

Surface morphologies were analysed under a scanning electron microscope (SEM) model Quanta FEG 250 (USA) equipped with EDX.

3. Results and Discussion

3.1. Off-grid battery charging

3.1.1. Off-grid charging profile

Figure 3 shows the test results for battery charging in the off-grid battery charging system. In agreement with previous studies [51–53], figure 3 displays that the charging process of lead acid batteries is complicated and passes through many stages. The charging process traverses three stages with two turning points. The initial stage is called constant-current charge during which the battery accepts all the applied charging current allowing the voltage to increase. The following stage is called the topping charge. This stage begins when the battery reaches saturation and starts to accept a small portion of the applied charging current. During this stage, the charge accepted by the battery starts to decline and the potential is kept at around 14.2 with slight fluctuation due to measurement noise. In the last stage, the current stabilized at a very low level.

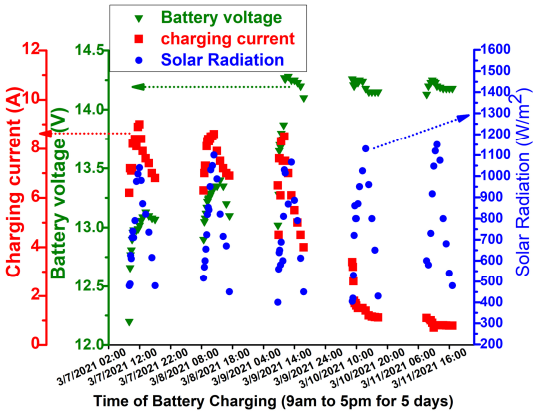

Figure 3: Battery charging behavior in an off-grid (PV) system at C/25.

3.1.2. Off-grid charging efficiency

A better representation of the charging stages is displayed in Figure 4 which reveals the progress of SOC and charging efficiency within each stage. During charging, SOC is represented by equation 1 [65]:

$$\mathbf{SOC} = \mathbf{SOC_o} + \left[\frac{\mathbf{1}}{\mathbf{C_n}} \int_{\mathbf{0}}^{\mathbf{t}} \pm \mathbf{I_{bc}} \,.\, \mathbf{dt}\right] \times \mathbf{100} \qquad (\mathbf{1})$$

Here, SOC_o denotes the SOC before charging in percentage for a battery with nominal capacity C_n in amp-hours. I_{bc} represents the battery current during charging in amperes and t is the charging time.

Charge efficiency represents the capacity losses throughout the charging process. It can be measured as the percent of the actual capacity accepted by the battery to the capacity transferred to it from the charging unit. The first stage of the charging process ends when the battery reaches about 85% SOC with a charge efficiency of 100%. This stage requires approximately 14 hours in our case (56% of the ideal charging time of C/25). Beyond 85% SOC, a fast decline in the charging efficiency is observed. This stage requires approximately 4 hours for the charge efficiency to decrease to 20%. Indeed, in the final stage of the charging process, when the battery SOC% exceeds 90%, the battery is stabilized and slowly approaches a fully charged state, characterized by low charging efficiency values (20-10%). As the battery nears its full capacity (>98% SOC), the charging efficiency naturally decreases. At this stage, the charging process becomes inefficient and impractical for real use. This decline in charging efficiency can be attributed to factors such as increased internal resistance, increased acid concentration, and the occurrence of reactions like oxygen evolution. These factors affect the battery's ability to accept and store additional charge. Consequently, charging the battery beyond 90% is not effective. These results bear a close resemblance to previous studies [51–53), further validating their reliability and consistency.

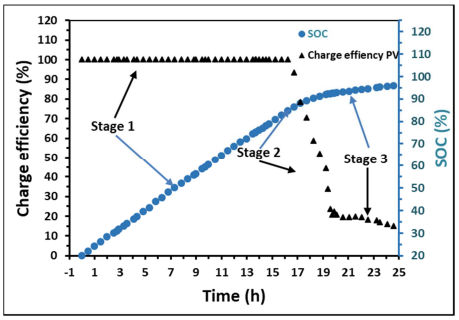

Figure 4: The variation of SOC% with time for 200 Ah Sonnenschein battery during charging from PV modules.

The growth and solvation of lead sulfate significantly impact the voltage, state of charge (SOC) percentage, and charging efficiency during the cycling process of lead-acid batteries. During the charging process, lead sulfates are transformed to pure lead at the cathode and lead peroxide at the anode liberating sulfuric acid into the electrolyte as mentioned in equation 2.

$$\mathbf{PbSO_4 + 2H_2O + 4e^- \rightarrow PbO_2 + 4H^+ + SO_4^{2-}} \qquad (\mathbf{2})$$

The battery voltage (V) is given by the equation 3.

$$\boldsymbol{V} = \boldsymbol{V_o} + \mathbf{I} \times \mathbf{R} \qquad (\mathbf{3})$$

Where V is the battery voltage throughout charge or discharge, Vo is the battery voltage at steady state or the open circuit voltage; and R is the internal resistance. I is the current delivered from and to the battery.

According to the electrochemical series, the theoretical cell voltage for a lead acid battery is approximately 2 V and exceeds 2.2 V due to overvoltage [54–58]. The deviation of the terminal voltage of a battery from its electromotive force (EMF) arises from the overvoltage and ohmic voltage drop causing the polarization effect. The ohmic voltage drop results from the resistances between battery components like the active materials, the porous separators, and the supportive grids. Overvoltage effects express the excess energy required for driving the electrochemical reaction at a certain rate [29, 59]

Figure 5 illustrates the growth of lead sulfate crystals for an old lead acid battery. The battery used in our study is a commercial one. The crystals were identified by EDX data, showing an atomic percent for Pb:S:O of approximately 1:1:4. This confirms the presence of lead sulfate, consistent with the expected stoichiometry for $PbSO_4$.The sulfate crystals seem to be not efficiently dissolved upon charging during cycling of the batters which participate in lowering the battery performance with time.Incomplete charges and partial state of charge operation (PSOC) prevent the proper dissolution of these crystals, leading to reduced charge acceptance, efficiency, and expedited battery failure. Hence, preventing irreversible sulfation is crucial in managing stationary lead-acid systems that change frequently. During the charging process, a battery's energy storage capacity decreases as its voltage increases. This occurs because lead sulfate on the electrode surface breaks down, dissolves, and releases sulfate

ions into the electrolyte. The greater the numbers of sulfate ions present in the electrolyte, the more intense the repulsion between the deposited ions and the incoming ones. The concentration of ions in the electrolyte, which is measured by the battery's state of charge (SOC), reflects this effect. A higher ion concentration corresponds to a higher SOC. Consequently, an increase in battery voltage leads to a higher SOC, resulting in a reduced capacity to store energy [60].

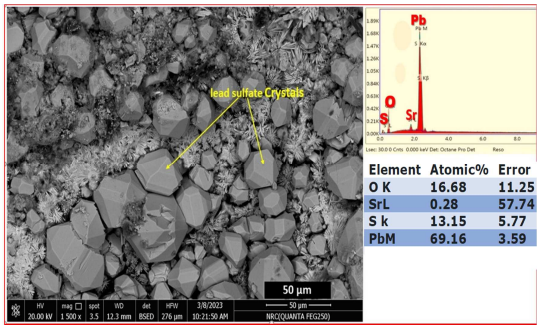

Figure 5: SEM and EDX images for lead sulfate crystals growth in old lead-acid battery.

3.2. Battery charging model

3.2.1. Thévenin battery model

The first order Thévenin battery model, named a one-time constant model, is an uncomplicated method for estimating the battery voltage behavior. It is an improvement to the earlier ECMs [30–33]. Figure 6 symbolizes the Thévenin battery model EC. It represented the battery terminal voltage (U_b) by a simple voltage source (U_{oc}), an internal resistance (R), and a parallel capacitor-resistor section (R1//C1). Uoc signifies the open circuit or the no-load voltage of the battery. R1, the polarization resistance, signifies the contact resistance amid the surface of the plates and the electrolyte. C1, the polarization capacitance, acts for the capacitance linking the parallel plates. The Thévenin model was designed to reflect the dynamic characteristics of the battery in the form of a polarization voltage by adding the R//C components [26, 28, 61].The main limitation of this model is that all the parameters are treated as constants however they are battery dependent [20, 50, 62, 63]. Besides, [19, 20, 28, 63] not account for the influence of SOC on the battery's voltage. However, these parameters are not consistently constant and vary based on several factors such as SOC, capacity, charging/discharging speeds, aging process, and temperature [31, 64].

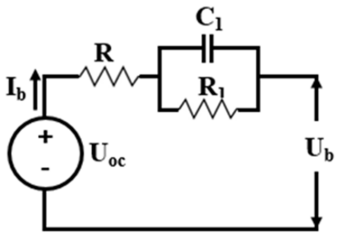

Figure 6: Equivalent circuit for the Thévenin model.

3.2.2. An improved Thévenin battery model

A more precise Thévenin battery model (shown in Figure 7) has been developed to accurately depict battery behavior by accounting for dynamic nonlinear characteristics. This enhanced model characterizes the EC parameters (the resistors and capacitors in addition to the on-load voltage) as SOC-dependent variables. Additionally, it separately specifies the charging and discharging processes [46, 61, 65], as illustrated in Figure 6. R_c, R_{1c}, and C_{1C} symbolize the EC parameters during the charging process, and R_d, R_{1d}, and C_{1d} are the EC parameters during the discharging process. The nonlinearity of the EC parameters and the separation between the processes of charging and discharging provide a more reliable framework for simulating the battery performance in real-world scenarios across various operating conditions [26, 39-40].

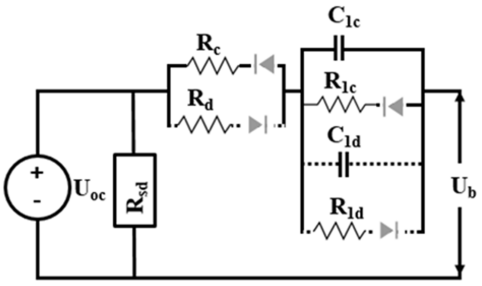

Figure 7: Improved Thévenin model for lead-acid battery.

The improved Thévenin model is an expansion of the traditional Thévenin model. This model represents the battery dynamic approach by considering the nonlinear behavior of the EC electric parameters. Regarding the proposed equivalent circuit, the terminal battery voltage during charging (U_{bc}) can be expressed according to the following equations.

$$U_{bc} = U_{oc} + I_b R_c + I_b R_{1c} \cdot \left[1 - e^{\left(-\frac{t}{R_{1c} \cdot C_{1c}}\right)}\right] \quad (4)$$

Where U_{bc} stands for the terminal voltage during charging, U_{oc} signifies the open circuit voltage. The

last term in the equation represents Uov which symbolizes the overvoltage through the resistor-capacitor section (R_{1c}//C_{1c}).

3.2.3. On-grid battery charging procedure

Figure 8 displays the battery voltage recorded during pulse charge tests from the electricity grid at a charging rate equivalent to about C/25 in a SOC interval ranging from 20 to 90%. U_{bc} and I_{bc} represent the terminal battery voltage and the charging current during the pulse charge process, respectively. The inset magnifies the battery terminal voltage upon pulsed charging. It highlights the distinct stages that voltage bath through during both the charging and rest processes. It gives a brief imagination about the concentration polarization and the steady state regions upon pulsed charging. The inset shows three stages. Firstly, a rapid potential decreases immediately after removing the charging source, referred to as the IR jump stage is observed. This stage reflects the influence of the battery's internal resistance (R) and its effect on the voltage response. Afterward, the potential decreased gradually due to the diffusion effect. This stage was labeled as U_{ov} in the inset and signified by a parallel capacitor-resistor section (R_{1c}//C_{1c}) in the EC. The last stage is the open circuit voltage recorded at the steady state and labeled as Uoc.

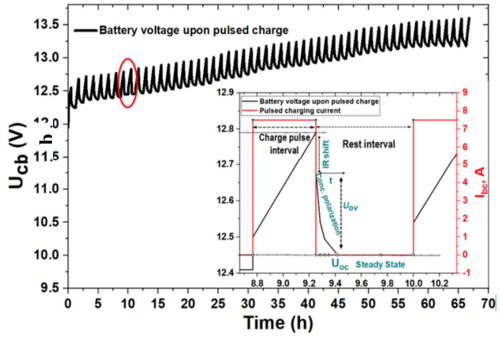

Figure 8: Pulse charging at C/25 for 200 Ah Lead-acid battery from 20% to 100% SOC and the inset represents the magnification details of the rest interval.

3.2.4. Parameters identification

As mentioned before, the non-linear behavior of the EC's parameters was determined as a function of the SOC, where the battery voltage and charging current were recorded when subjected to successive charge and rest steps. The fitted equations were implemented in the investigated model as follows.

The equ ation of the simulated battery voltage is derived from the EC postulated for the selected model. Additionally, the battery modeling equations are mainly based on the SOC which is quantified as a percentage.

- ***Open circuit voltage (Uoc)***

U_{oc} was measured when the battery reached the steady state close to the end of the rest intervals in the charging test. Figure 9a displays the plot of U_{oc} and SOC and their fitted curves. The experimental data are represented by black dots, while the black line represents its fitted curve. Although it is commonly believed that the relationship between $\boldsymbol{U_{oc}}$ and SOC follows a linear trend [46,65], our research indicates otherwise [66]. Better approximation has been achieved by considering nonlinear relation and a quadratic polynomial fitting equation was used to approximately represent the relationship between U_{oc} and SOC, represented by Equation 5.

$$\mathbf{U_{OC}} = \mathbf{a}_o + \mathbf{b}_o.\mathbf{SOC} + \mathbf{d}_o.\mathbf{SOC}^2 \quad (5)$$

Where a_o, b_o, and d_o are constants and equal 12.9, 0.0007, and 0.0001, respectively.

- ***Series resistance (Rc) identification:***

R_c is determined from the rapid decline in potential in the first stage of the recovery interval. It represents the resistance of the electrolyte and battery plates. Figure 9b illustrates the change of R_c as a function of the SOC. Our study successfully approximated the experimental R_c values through exponential fitting, resulting in equation 6.

$$\boldsymbol{R_c} = \boldsymbol{e}^{(\mathbf{a_1}+\mathbf{b_1}.\mathbf{SOC}+\mathbf{d_1}.\mathbf{SOC^2})} \quad (6)$$

Where a_1, b_1 and d_1 are constants and equals -3.95, -0.0255, and 0.00036, respectively.

- ***R//C components:***

The parameters of the R//C section were estimated from the recorded voltage variation (U_{ov}) during recovery periods following the charging steps in the second stage, as illustrated in Figure 7. It is anticipated that the transients associated with the charge steps will dissipate within 5 minutes, based on settling time (t) estimation. The time constant (τ) measures the ability of the system to step to a certain fraction of its final value, usually 63.2%. According to Figure 5, it approximately takes one minute for the voltage to reach 63.2% of its steady state value during the recovery stage. Thus, the capacitance ($\mathbf{C_{1c}}$) is determined according to equation 7 as mentioned below:

$$\mathbf{C}_{1c} = \frac{\boldsymbol{t}}{\mathbf{5}\boldsymbol{R_x}} = \frac{\boldsymbol{\tau}}{\boldsymbol{R_x}} \quad (7)$$

Where, $\boldsymbol{\tau} = \frac{t}{5}$

$\boldsymbol{\tau}$: A time constant in seconds

$\mathbf{R}_x$ displays the resistance of the battery circuit during charge ($\mathbf{R_o}$ and $\mathbf{R_{ov}}$) and is calculated in equation 8:

$$R_x = \frac{R \times R_{1c}}{R + R_{1c}} \qquad (8)$$

Figures **9c** and **d** display the dependence of the parameters of the R//C section (R_{1c} and C_{1c}) on SOC. Utilizing curve-fitting analysis, $\mathbf{R}_{Ic}$ and $\mathbf{C}_{Ic}$ can be expressed as:

$$\mathbf{R_{1c}} = \begin{cases} \mathbf{a_2 + b_2 \times SOC}\ , & \mathbf{SOC \leq 70} \\ \mathbf{a_3 + b_3 \times SOC + d_3 \times SOC^2}\ , & \mathbf{SOC > 70} \end{cases} \qquad (9)$$

$$\mathbf{C_{1c}} = \begin{cases} \mathbf{a_4 + b_4 \times SOC + d_4 \times SOC^2}\ , & \mathbf{SOC \leq 70} \\ \mathbf{a_5 + b_5 \times SOC}\ , & \mathbf{SOC > 70} \end{cases} \qquad (10)$$

Where a_2, b_2, a_3, b_3, d_3, a_4, b_4, d_4, a_5 and b_5 are constants and their values are shown in table 1.

Table 1: Values of a_2, b_2, a_3, b_3, d_3, a_4, b_4, d_4, a_5 and b_5 as the fitting constants

a_2	b_2	a_3	b_3	d_3
0.0261	0.0003	0.967	-0.0246	0.00017
a_4	b_4	d_4	a_5	b_5
89	1.328	-0.022	206	-1.855

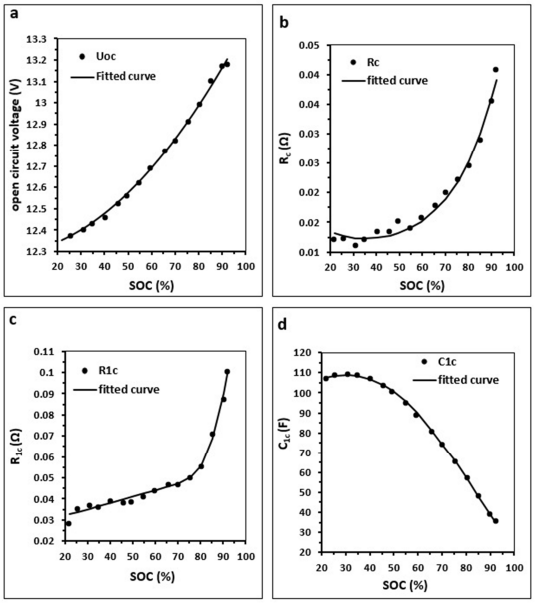

Figure 9: The variation of the experimental data (black dots) of the electric circuit parameters (**a**) the open circuit voltage (U_{oc}), (**b**) internal resistance (R_c), (**c**) the series resistance (R_{1c}), and (**d**) the series capacitance (C_{1c}) with SOC and their fitted curves (black line).

3.2.5. Model Validation

Figure 10 represents the effectiveness of the improved Thévenin model. It displays the validity of the model by comparing the actual experimental battery voltage with the simulated one. The improved Thévenin model can successfully simulate the overall battery behavior during charging with an RMSE% =1%.

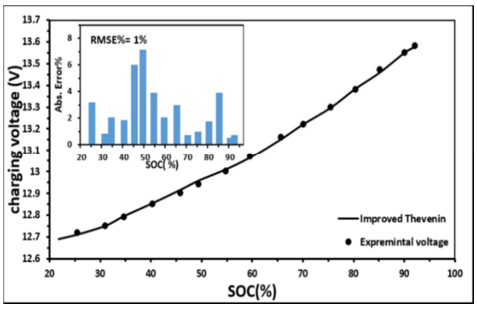

Figure 10: Comparison between the terminal battery voltage recorded during charging (black dots) and the terminal voltage predicted via the improved Thévenin model (black line).

4. Conclusion:

The charging process and charge efficiency of lead-acid batteries across a wide range of states of charge up to 100% SOC were extensively studied. It was observed that charging the battery to a level higher than 90% SOC proved to be ineffective, in line with findings from previous studies. Additionally, the modeling of charging using electric circuit models and their validation involved assessing model parameters as a function of SOC using curve fitting techniques. This allowed for an accurate representation of battery performance while maintaining model simplicity and enhancing model topology by establishing an accurate relationship between battery capacity or SOC and voltage. To further enhance the ECMs model topology, a modified Thévenin model was experimentally validated on a 200 Ah lead acid battery at full charging (approximately 100% SOC), resulting in improved accuracy concerning the relationship between battery capacity or SOC and voltage. The validation resulted in a RMSE of around 1%, indicating that this model effectively captures battery behavior across its entire operating range.

5. *Conflicts of interest*: The authors declare that they have no conflict of interest in this article.

6. Acknowledgments

E. T. El Shenawy acknowledges the financial support of this work by the National Research Centre project (13040111)

7. Abbreviations

Equivalent circuit model	ECM
equivalent circuit	EC
state of charge	SOC
parallel capacitor-resistor section	(R//C)
terminal battery voltage during charging	U_{bc}
battery charging current	I_{bc}
Open circuit voltage	U_{oc}
battery's internal resistance	R_o

8. References

1. Bahgat, A., Helwa, N., Ahamd, G., & El Shenawy, E. Estimation of the maximum power and normal operating power of a photovoltaic module by neural networks. Renewable Energy. 2004; 29(3), 443-457.
2. Khattab N, Badr M, Maalawi K, El Shenawy E, El Ghetany H, Ibrahim M. Hybrid renewable energy system for water desalination: A case study for small green house hydroponic cultivation in Egypt. ARPN Journal of Engineering and Applied Sciences. 2016; 11(21) 12380-12390.
3. Abdo, R. M., Hegazy, A., El Shenawy, E. T., El Sherbini, E. Modelling of the dynamic behavior for Lead-Acid Batteries in photovoltaic systems. Egyptian Journal of Chemistry, 2024; 67(13): 27-36.
4. Sweelem E, El Shenawy E, Abd El-Shafy A. Effect of Different Dust Accumulation on the Performance of PV Module in Egypt. Effect of Different Dust Accumulation on the Performance of PV Module in Egypt. International Journal of Advanced Information Science and Technology. 2015; 44(44).
5. Khattab NM, Badr MA, El Shenawy ET, Sharawy HH, Shalaby MS. Economic Analysis of Stand-Alone Hybrid Wind/PV/Diesel Water Pumping System: A Case Study in Egypt. In: Modeling, Simulation and Optimization of Wind Farms and Hybrid Systems. 2020. p. 205–23.
6. Bahgat ABG, Helwa NH, Ahmad GE, El Shenawy ET. Maximum power point traking controller for PV systems using neural networks. Renew Energy. 2005;30(8):1257–68.
7. Ahmad GE, El Shenawy ET. Optimized photovoltiac system for hydrogen production. Renew Energy. 2006;31(7):1043–54.
8. El Shenawy ET, Hegazy AH, Abdellatef M. Design and optimization of stand-alone PV system for Egyptian rural communities. International Journal of Applied Engineering Research. 2017;12(20):10433–46.
9. Vergori E. Battery Modelling and Simulation Using a Programmable Testing Equipment. Computers. 2018;7:20.
10. Mansuroglu A, Gencten M, Arvas MB, Sahin M, Sahin Y. Investigation the effects of chlorine doped graphene oxide as an electrolyte additive for gel type valve regulated lead acid batteries. Journal of Energy Storage. 2023; 64:107224.
11. Díaz-Pilpe J, Maldonado-Galarza F, Helguero C, Ramírez E, Ben Rejeb H, Zwolinski P, Hidalgo-Crespo J, Amaya-Rivas J . Methodology for the third-party reconditioning process of automotive vented lead-acid (VLA) batteries. Procedia CIRP. 2023; 118:970–5.
12. Mohsin M, Picot A, Maussion P. A new lead-acid battery state-of-health evaluation method using electrochemical impedance spectroscopy for second life in rural electrification systems. J Energy Storage, 2022; 52:104647.
13. Tsafack P, Fru SE, Nghemachi AV, Tanyi E. Impact of high constant charging current rates on the charge/discharge efficiency in lead acid batteries, for residential photovoltaic system applications. J Energy Storage. 2023; 63:107013.
14. Festijo ED, Juanico DEO, Nonat P V., Galapia X, Malab KMS. Acoustic non-invasive estimation of lead–acid battery state of health: Applications for cell-level charge balancing. Energy Reports. 2022; 8:372–7.
15. Nodeh ZP, Beni AA, Moghadam AJ. Development of evaporation technique for concentrating lead acid wastewater from the battery recycling plant, by nanocomposite ceramic substrates and solar/wind energy. Journal of Environmental Management. 2023;328:116980.
16. Letcher TM. Storing electrical energy. In: Managing Global Warming: An Interface of Technology and Human Issues; 2019: 365–77.
17. Lopes PP, Stamenkovic VR. Past, present, and future of lead–acid batteries. Science. 2020;369(6506):923–4.
18. Chen H. Electrolytes of lead-acid batteries. In: Lead-Acid Battery Technologies: Fundamentals, Materials, and Applications. 2015. p. 137–62.
19. Moubayed N, Kouta J, El-Ali A, Dernayka H, Outbib R. 33rd IEEE Photovoltaic Specialists Conference, San Diego, CA, USA, 2008.
20. Saldaña G, SanMartín JI, Zamora I, Francisco Javier Asensio, Oñederra O. Analysis of the Current Electric Battery Models for Electric Vehicle Simulation. Energies (Basel). 2019;12(14):2750.
21. Jackey RA. A simple, effective lead-acid battery modeling process for electrical system component selection. SAE Transactions. 2007:219-27.
22. Copetti JB, Lorenzo E, Chenlo F. A general battery model for PV system simulation. Progress in Photovoltaics: Research and Applications. 1993;1(4):283–92.
23. Mu H, Xiong R. Modeling, evaluation, and state estimation for batteries. In Modeling, Dynamics and Control of Electrified Vehicles. 2018:1-38.
24. Pattipati B, Sankavaram C, Pattipati KR. System identification and estimation framework for pivotal automotive battery management system characteristics. IEEE Transactions on Systems, Man, and Cybernetics, Part C (Applications and Reviews). 2011;41(6):869–84.
25. Shi M, Yuan J, Dong L, Zhang D, Li A, Zhang J. Combining physicochemical model with the

equivalent circuit model for performance prediction and optimization of lead-acid batteries. Electrochim Acta. 2020;353:136567.
26. Bašić M, Vukadinović D, Višnjić V, Rakić I. Dynamic equivalent circuit models of lead-acid batteries–a performance comparison. IFAC-Papers online. 2022. 1; 55(4): 189-94.
27. Zhou W, Zheng Y, Pan Z, Lu Q. Review on the Battery Model and SOC Estimation Method. Processes. 2021. 20;9(9):1685.
28. Lavety S, Keshri RK, Chaudhari MA. A dynamic battery model and parameter extraction for discharge behavior of a valve regulated lead-acid battery. J Energy Storage. 2021 Jan 1; 33:102031.
29. Berndt D. Maintenance-Free Batteries: Lead-Acid, Nickel/Cadmium, Nickel/Metal Hydride (Electronic & Electrical Engineering Research Studies). 2nd Edition. 1997:1–520.
30. Kim YH, Ha HD. Design of interface circuits with electrical battery models. IEEE Transactions on Industrial Electronics. 1997; 44(1): 81–6.
31. Jongerden MR, Haverkort BR. Battery modeling. Centre for Telematics and Information Technology, University of Twente, Technical Report TR-CTIT-08-01. 2008.
32. Gold S. A PSPICE macromodel for lithium-ion batteries. InThe twelfth annual battery conference on applications and advances 1997;14 : 215-222. IEEE.
33. Hageman SC. Simple PSpice models let you simulate common battery types. Electronic Design News (EDN). 1993;38(22):117–29.
34. Darabi A, Hosseina M, Gholami H, Khakzad M. Modeling of lead-acid battery bank in the energy storage systems. International Journal of Emerging Technology and Advanced Enegineering. 2013; 3(3):4–9.
35. Ganesan, A. and Sundaram, S.,. *A heuristic algorithm for determining state of charge of a Lead Acid Battery for Small Engine Applications* (No. 2012-32-0082). SAE Technical Paper; 2012 Oct 23.
36. Fang H, Zhao X, Wang Y, Sahinoglu Z, Wada T, Hara S, et al. State-of-charge estimation for batteries: A multi-model approach. In: 2014 American Control Conference. IEEE; 2014. p. 2779–85.
37. Coupan F, Sadli I, Marie-Joseph I, Primerose A, Clergeot H. New battery dynamic model: Application to lead-acid battery. In 2010 The 2nd International Conference on Computer and Automation Engineering (ICCAE) 2010; 5:140-145. IEEE.
38. Salameh ZM, Casacca MA, Lynch WA. A mathematical model for lead-acid batteries. IEEE Transactions on Energy Conversion. 1992;7(1):93–8.
39. Li A, Pelissier S, Venet P, Gyan P. Fast Characterization Method for Modeling Battery Relaxation Voltage. Batteries. 2016 6;2(2):7.
40. Hu Y, Yurkovich S, Guezennec Y, Yurkovich BJ. A technique for dynamic battery model identification in automotive applications using linear parameter varying structures. Control Engineering Practice. 2009;17(10):1190–2010.
41. Jiang S. A parameter identification method for a battery equivalent circuit model. SAE Technical Paper; 2011.
42. Hidalgo-Reyes JI, Gómez-Aguilar JF, Escobar-Jiménez RF, Alvarado-Martínez VM, López-López MG. Classical and fractional-order modeling of equivalent electrical circuits for supercapacitors and batteries, energy management strategies for hybrid systems and methods for the state of charge estimation: A state of the art review. Microelectronics Journal. 2019. 1;85:109–28.
43. Calborean A, Murariu T, Morari C. Optimized lead-acid grid architectures for automotive lead-acid batteries: An electrochemical analysis. Electrochim Acta. 2021. 10;372:137880.
44. Sadabadi KK, Ramesh P, Tulpule P, Guezennec Y, Rizzoni G. Model-based state of health estimation of a lead-acid battery using step-response and emulated in-situ vehicle data. Journal of Energy Storage. 2021. 1;36:102353.
45. Lee S, Cherry J, Safoutin M, McDonald J. Modeling and Validation of 12V Lead-Acid Battery for Stop-Start Technology. SAE Technical Papers; 2017.
46. Haddad R, Shahat A El, Kalaani Y. Lead Acid Battery Modeling for PV Applications. Journal of Electrical Engineering. 2015;15(2):17–24.
47. Loukil J, Masmoudi F, Derbel N. A real-time estimator for model parameters and state of charge of lead acid batteries in photovoltaic applications Journal of Energy Storage. 2021.1; 34:102184.
48. Bolsi PC, Prado EO, Lima ACC, Sartori HC, Pinheiro JR. Battery autonomy estimation method applied to lead–acid batteries in uninterruptible power supplies. Journal of Energy Storage. 2023;58:106421.
49. Huck M, Sauer DU. Modeling transient processes in lead-acid batteries in the time domain. Journal of Energy Storage. 2020;29:101430.
50. Cui WH, Wang JS, Chen YY. Equivalent circuit model of lead-acid battery in energy storage power station and its state-of-charge estimation based on extended kalman filtering method. Engineering Letters. 2018;26(4):504–17.
51. Cugnet M, Liaw BY. Effect of discharge rate on charging a lead-acid battery simulated by mathematical model. J Power Sources. 2011;196(7):3414–9.
52. Krope J, Olabi AG, Goričanec D, Božičnik S. Smart Solar Battery Charger for PV-Application. In10TH International Conference on Sustainable Energy and Environmental Protection Renewable Energy Sources. 2017:45.
53. Huang BJ, Hsu PC, Wu MS, Ho PY. System dynamic model and charging control of lead-acid battery for stand-alone solar PV system. Solar Energy. 2010;84(5):822–30.
54. Kosky P, Balmer R, Keat W, Wise G. Electrochemical Engineering. In: Exploring Engineering (Fifth Edition) An Introduction to Engineering and Design. 2021: 383–403.
55. Akinbulu IA, Ogunbayo BT. Thermodynamics of electrochemical reaction in Lead- acid Battery. Journal of Research and Reviews in Science. 2018;5:87–91.

56. Takehara ZI. On the reaction in the lead-acid battery (as the special review-article by the 2005'Gaston Plante Medal recipient). Journal of Power Sources. 2006;158(2):825-30.
57. Torabi F, Ahmadi P. Lead–acid batteries. In: Simulation of Battery Systems. Elsevier; 2020. p. 149–215.
58. Groot DR, van der Linde JA. The processing of eWaste. Part 2. The electrochemical leaching behaviour of a metallic alloy derived from waste printed circuit boards. Journal of The Southern African Institute of Mining and Metallurgy. 2009;109(12):701–7.
59. Jantharamin N, Zhang L. A new dynamic model for lead-acid batteries. IET Conference on Power Electronics, Machines and Drives, York, 2008:86–90.
60. Catherino H, Feres F, Trinidad F. Sulfation in lead–acid batteries. Journal of Power Sources. 2004;129(1):113-120
61. Dürr M, Cruden A, Gair S, McDonald JR. Dynamic model of a lead acid battery for use in a domestic fuel cell system. Journal of Power Sources. 2006;161(2):1400–11.
62. Sobczak MMSJ. Development of an algorithm for estimating Lead-Acid Battery State of Charge and State of Health . MSc, thesis. 2013.
63. Chan HL, Sutanto D. A new battery model for use with battery energy storage systems and electric vehicles power systems. 2000 IEEE Power Engineering Society, Conference Proceedings. 2000;1(c): 470-475.
64. Jongerden MR, Haverkort BR. Which battery model to use ? IET Software. 2009;3(6):445–57.
65. Jantharamin N, Zhang L. A new dynamic model for lead-acid batteries. In: 4th IET International Conference on Power Electronics, Machines and Drives (PEMD 2008). IEE; 2008. p. 86–90.
66. Yu Y, Narayan N, Vega-Garita V, Popovic-Gerber J, Qin Z, Wagemaker M, Bauer P, Zeman M. Constructing accurate equivalent electrical circuit models of lithium iron phosphate and lead-acid battery cells for solar home system applications. Energies. 2018;11(9):2305.